Highly Efficient Miniaturized Magnetorheological Valves Using Electropermanent Magnets

Sofia Lydia Ntella, Adrien Thabuis, *Student Member, IEEE*, Bhawnath Tiwari, Kenny Jeanmonod, Christian Koechli, and Yves Perriard, *Senior Member, IEEE*

***Abstract*—Fluidic systems enable actuation in various applications, such as automotive, medical, and industrial robotics. Miniaturized valves constitute a fundamental controlling element of modern fluidic systems, intriguing the interest of many researchers. This letter presents the design, implementation, and experimental validation of a miniaturized magnetorheological valve. The valve is highly efficient due to its capability of sustaining high loads with low energy consumption. This work includes the estimation strategy for the sustained load. Magnetorheological fluid is used both as an actuation fluid and as control medium. The inner iron core of the traditional magnetorheological valve is replaced with an AlNiCo-5 rod. The latter provides the possibility of magnetic energy storage, without continuous power supply. This changes the actuation mechanism from an electromagnet to an electropermanent magnet. The valve's capability to sustain pressure up to 1010 kPa, for a volume of 353 mm^3, is demonstrated experimentally. The fluid flow rate when the valve is open is 459 mm^3/s for a pressure difference of 993 kPa. The corresponding power consumption is negligible in steady-state condition, while consuming 15.3 mJ when activated and 6 mJ when deactivated. The experimental results also validate the possible tunability of the pressure sustaining capability of the valve.**

***Index Terms*—Hydraulic/pneumatic actuators, mechanism design.**

I. Introduction

POWER transmission is omnipresent in engineering. It involves the conversion of energy into different forms and its distribution to different systems. This can be achieved with electrical, mechanical, or fluid technologies. Among them, fluid power transmission systems present the advantages of high power-to-weight ratio [1], ability to handle high-magnitude forces and torques compared to mechanical transmissions [2], and increased heat transfer capability [3]. There exist mainly two types of fluid systems, the hydraulic ones that employ incompressible liquids such as oil, water or other types of fluids; and the pneumatic ones that utilize neutral gases such as air. Due to the aforementioned advantages, fluidic-system-based power transmission is exploited in a wide range of applications. In addition to the construction field and driving mobile machinery [4], hydraulic systems are key components in robotic manipulators, playing an important role in the automation of industrial activities [5]. In automotive systems, clutches [6] or vehicle suspensions, which are vital for comfort and safety, are actualized by fluidic actuators [7]. While primarily controlling large-scale motion, pneumatic and hydraulic soft actuators are getting miniaturized. A great showcase is minimally invasive surgery [8] and rehabilitation systems [9], enabled by fluidic technologies that use miniaturized valves.

Valves constitute an integral component for the control of fluid direction and flow rate in fluidic systems. Numerous attempts have been made in the last decades to further enhance the capabilities of valves through the use of different principles. Solenoid valves have been used as an inexpensive and accurate solution [10], [11], [12], [13], as well as active mechanical valves based on thermal [14], [15], or elastomeric principle [16], [17]. Valves based on Dielectric Elastomer Actuators (DEAs) have been developed recently to achieve lightweight and compact fluidic regulation systems [18]. Furthermore, electrorheological fluid (ERF) [19], [20] and magnetorheological fluid (MRF), two types of smart materials, have been used as pressurized liquids in fluidic valves for applications such as automotive or medical [21], [22], [23], [24], [25]. ERFs and MRFs are characterized by a controllable, reversible change of viscosity with the application of an external electric or magnetic field respectively. As a result, they allow the creation of valves with simple structure and fast response when supplied constantly with DC current and voltage. In addition, both permanent magnet (PM) and electropermanent magnet (EPM) have been employed in valves for pneumatic systems due to advantages of low power consumption, compactness and minimal weight [26], [27]. The advantages of EPMs have also been exploited in actuation applications different from valves, such as latching mechanisms in self-assembled robots [28], [29]. Finally, the addition of EPM technology in MRF valves has paved the way for miniaturized MRF valves that overcome the constraint of steady-state power supply and allow low energy functionality [30], [31].

Fig. 1 depicts a comparative plot of the various principles mentioned previously, on a logarithmic scale for clarity. It shows the maximum reported pressure sustained by the valves with regard to their volume. Besides, the representation of several

Manuscript received 9 September 2022; accepted 4 January 2023. Date of publication 20 January 2023; date of current version 3 February 2023. This letter was recommended for publication by Associate Editor G. Endo and Editor J. P. Desai upon evaluation of the reviewers' comments. This work was supported by Swiss National Science Foundation (SNSF) and Innosuisse-Swiss Innovation Agency through BRIDGE funding Programme under Grant 20B2-1_181020. *(Sofia Lydia Ntella and Adrien Thabuis, contributed equally to this work.) (Corresponding author: Yves Perriard.)*

The authors are with the Integrated Actuators Laboratory, École Polytechnique Fédérale de Lausanne, 2000 Neuchâtel, Switzerland (e-mail: sofia.ntella@epfl.ch; adrien.thabuis@epfl.ch; bhawnath.tiwari@epfl.ch; kenny.jeanmonod@epfl.ch; christian.koechli@epfl.ch; yves.perriard@epfl.ch).

Digital Object Identifier 10.1109/LRA.2023.3238669

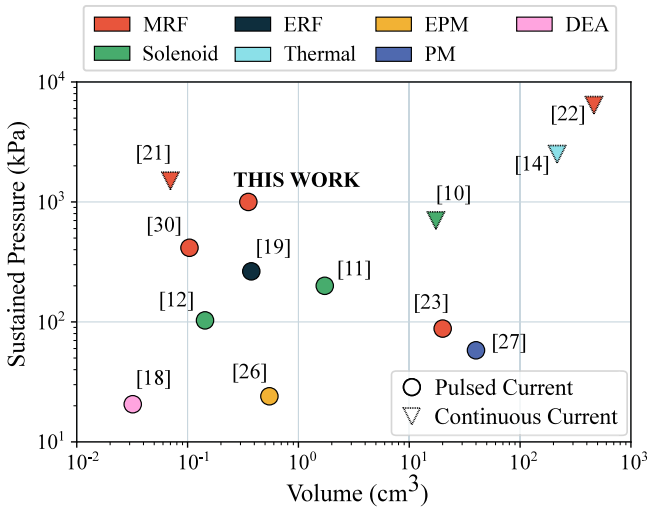

Fig. 1. Comparison of different valves depending on their physical driving principle, maximum sustained pressure, and size.

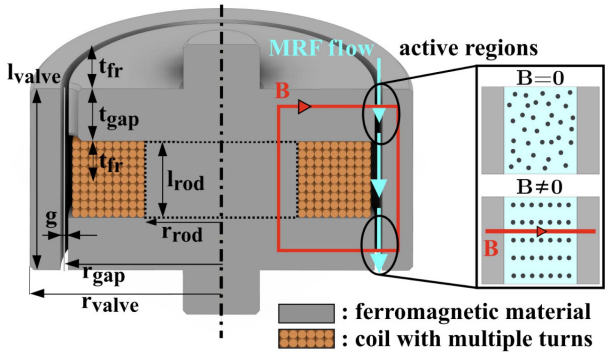

Fig. 2. Cut view of a conventional annular MR valve with dimensions. The MRF in the active regions is represented with and without a magnetic field.

works with circles and triangles differentiates them according to the activation principle and, thus, their power consumption. Working principles requiring continuous current for valve activation consume significant amounts of power and energy. On the contrary, valves activated with a single pulse of current, which is necessary only for switching from one state to the other, tend to consume negligible power in the steady state resulting in highly efficient systems. In Fig. 1, the size of the valve affects the maximum sustained pressure. The highest pressure is achieved in very high volumes. At the same time, valves that sustain more than 1100 kPa consume considerably higher power, due to the continuous activation current. On the other hand, the smallest-in-volume solutions, with negligible power consumption in the steady state, present very low sustained pressure. In automation applications, especially when dealing with soft robotic systems, miniaturized valves with low power consumption facilitate integration. Especially valves sustaining hundreds of kPa of pressure enable a wide range of motion and forces. Apart from these, the characteristic of tunability of the sustained pressure can attribute flexibility to the robotic systems. Finally, the flow rate is an important parameter defining the performance of valves. In valves with high volumes [11], [14], [22] flow rates higher than 73000 mm^3/s are reported. There also exist valves with low volume and high flow rate [18], [21], [26]. However, they either consume high energy due to continuous activation current [21] or sustain very low pressure when closed [18], [26].

This work proposes a miniaturized MRF valve with high efficiency in terms of sustained pressure and energy consumption, which incorporates an EPM. The proposed valve is designed for controlling hydraulic systems that use MRF as filling fluid. Its function is binary, operating either in the on-state, completely blocking the flow rate, or in the off-state, allowing the fluid flow. An analytical model in combination with simulation results are presented with the goal to estimate the pressure that the valve can withstand. The EPM is added in the traditional structure of the MRF valve with the goal to decrease its power consumption. This is achieved with a low-volume design, but with high sustained pressure capability. The above features make the proposed device an attractive solution for various applications such as control of soft bending actuators or medical devices with MR modules for plantar pressure offloading in diabetic patients [25].

The paper is organized as follows. Section II describes the design and working principle of traditional MRF valves without EPM and with EPM in the structure. In this section, the device is modeled analytically and simulated magnetically to define the pressure it can sustain. Section III provides the experimental setup and its principle, as well as the experimental results. The latter are compared with the analytical and numerical model. Finally, Section IV presents the conclusions and future perspectives.

II. Device Presentation

A. MRF Valve General Principle

MRF is a class of smart materials, comprising of micron-sized iron particles, dispersed in oil and enhanced by surfactants [32]. The traditional magnetorheological (MR) valve is cylindrical and consists of different parts. Firstly, a coil is wound around a ferromagnetic rod, as in Fig. 2. This part is covered by two ferromagnetic discs on the top and the bottom. Additionally, a cylindrical, ferromagnetic structure, is surrounding the first part. A gap is formed between the two structures, allowing the vertical flow of the MRF. The inner structure acts as an electromagnet. When the coil is supplied by a DC current, it imposes a magnetic flux density B in the active regions of the gap (Fig. 2). The flux density is perpendicular to the fluid flow in the active regions. Accordingly, the particles shape chain-like structures, aligned with the magnetic field lines. As a consequence, the MRF viscosity η in the active regions increases, and the fluid flow rate Q decreases. This results in an increase of the pressure difference ΔP developed between the two sides of the valve.

B. Electropermanent Magnet Principle

Our work proposes the use of an electropermanent H^i magnet (EPM) [33], instead of an electromagnet to impose the magnetic

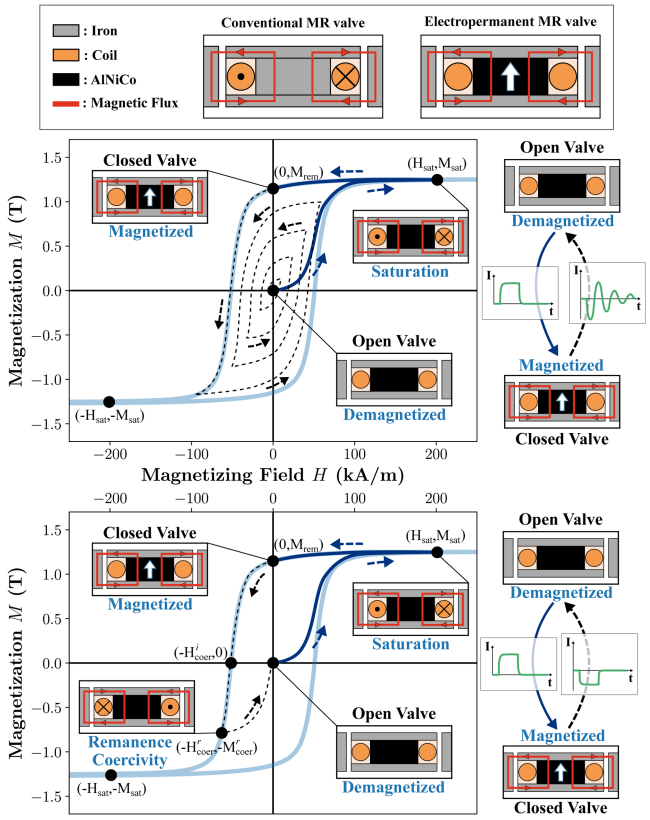

Fig. 3. Operation principle of the electropermanent MR valve based on an ideal M-H characteristic of a device made of AlNiCo-5. There are two different ways of demagnetizing the rod: a decaying oscillating external field (top), or a negative pulsed external field reaching the *remanence coercivity* of the material. The white arrow represents the magnetization direction of the rod.

flux density in the active regions of the valve. This is achieved by replacing the inner iron rod used in the conventional MR valve, with a magnetic rod with tunable magnetization. The coil is supplied continuously with current to activate the MRF in the standard valve to close it. Alternatively, in the proposed EPM valve, the coil is used in a pulsed manner to magnetize or demagnetize the inner magnetic rod, closing or opening the valve respectively. A careful choice of magnetic material is necessary to construct an EPM. In this application, it must be made of a ferromagnetic material with a large remanent magnetization and a low magnetizing field (i.e. *soft* ferromagnetic material). The fulfillment of the above specifications led to the choice the AlNiCo-5 material for our device.

Fig. 3 shows a schematic of the conventional and proposed valve. It also presents two possible operations of the new valve, which are illustrated on the magnetization curve (M-H characteristic) of the AlNiCo-5. The magnetizing field H, external to the material, is the one generated by the coil and is proportional to the ampere-turn product: $N \cdot I$, with N the number of turns of the coil, and I the electric current flowing through it. The resulting magnetization of the material M is defined as follows:

$$M = B - \mu_0 H = \mu_0 [\mu_{r(H)} - 1] \cdot H, \qquad (1)$$

with μ_0 the magnetic constant, and μ_r the relative magnetic permeability of the material. The non-linear relationship of the permeability with the magnetizing field $\mu_{r(H)}$, results in different magnetization for the same magnetizing field. Thus, such material shows hysteresis (i.e. the magnetization depends on its *history*). This, usually undesired behavior, is here harvested to operate the electropermanent magnet.

The inner rod in AlNiCo-5 is initially demagnetized ($H = 0, M = 0$), there is no magnetic field blocking the MRF and thus, the valve is open. When a positive electric current passes through the coil, the external magnetic field, in which the AlNiCo-5 is placed (i.e. magnetizing field), increases until reaching saturation ($H = H_{\text{sat}}, M = M_{\text{sat}}$). When the current supply to the coil stops, there is no more magnetizing field, and the material reaches its remanence ($H = 0, M = M_{\text{rem}}$). The remanent magnetization in the material makes it act as a permanent magnet. The valve is closed in this state.

There are two ways of demagnetizing a magnetic material. The first one is by applying a decaying oscillating external magnetic field [34], which enables reaching the origin of the M-H curve despite the hysteresis of the material and for any initial state of the material (its history). It is depicted on the top M-H curve of Fig. 3. The second method is by applying a negative external magnetic field so as to reach the *remanence coercivity* [35] ($H = -H^r_{\text{coer}}, M = -M^r_{\text{coer}}$) of the material, leading to a demagnetized state when the external field is removed. This should not be confused with the *intrinsic coercivity* corresponding to a null magnetization of the material under a specific external magnetic field ($H = -H^i_{\text{coer}}, M = 0$). Indeed, the hysteretic behavior of the material would result in a non-null remaining magnetization when the external magnetic field is removed. The *remanence coercivity* is a theoretical state arduously reached precisely in practice, preventing a perfect demagnetization. Nevertheless, the remaining magnetization can be considered small enough in many applications, such as this one. This method is preferred in this work because it requires a single demagnetization pulse implemented with a simple electronic design. If partial magnetization of the valve is desired (tunability of the sustained pressure as later explained), the first option should be considered as it is more robust and independent of the magnetization state.

Numerous works have presented electropermanent magnets [28], [29], [30], [31], [33], [36], [37] composed of two different ferromagnetic materials (i.e. magnets) placed in parallel with each other and between two iron pieces. In these cases, there is a *hard* material, such as NdFeB, and a *soft* material such as AlNiCo-5. The pulse of current through the coil affects only the *soft* material. The latter is always fully magnetized, either in one direction (same as the *hard* one), or in the other (opposed to the *hard* rod). The result is a device externally seen as magnetized or demagnetized respectively. The aforementioned combination of the two magnet types is necessary to prevent the self-demagnetization of the *soft* material (AlNiCo-5). In this work, the small air gap and the negligible change of magnetic permeability coming from the MRF flow prevent the self-demagnetization of the *soft* material. In this sense, there is no need for a *hard* material, but only the use

TABLE I
CHARACTERISTICS OF MRF VALVE AND ALNICO-5 MATERIAL PROPERTIES

Parameter	Value	Parameter	Value	Parameter	Value
g (mm)	0.18	l_{rod} (mm)	1.9	M_{rem} (T)	1.15
r_{gap} (mm)	4.09	h_{valve} (mm)	4.55	B_{rem} (T)	1.15
r_{valve} (mm)	5	V (mm^3)	353	H^i_{coer} (kA/m)	52.2
r_{rod} (mm)	2	L_c (μH)	61	H_{sat} (kA/m)	200
t_{gap} (mm)	1.325	R_c (Ω)	0.46	M_{sat} (T)	1.25
t_{fr} (mm)	0.32	N	55	B_{sat} (T)	1.50

of a single *soft* material (AlNiCo-5 in our case) is sufficient. To the authors' knowledge, there are only a few works, such as [38], that use a single AlNiCo-5 magnet inside an electropermanent magnet structure. There, despite taking advantage of the full magnetization curve, the large air-gap and varying magnetic environment will result in its self-demagnetization, jeopardizing a reliable operation. The strategy proposed in this paper is robust and highlights a great application of single-rod electropermanent magnets.

C. Analytical and Numerical Model

In this section, an analytical model of the device is derived. The goal is to determine the magnitude of the current pulse supplying the coil and to estimate the maximum pressure the valve can sustain. The chosen strategy to demagnetize the rod is to use a single negative pulse of current reaching the *remanence coercivity* of the material (as shown in Fig. 3). However, magnet manufacturers do not provide the characteristics of this state because it relies on highly non-linear phenomena and is dependent on the magnetization state as well as on the rod environment. Thus, the negative current I^i_{coer} needed to reach the *intrinsic coercivity* is derived. It will serve as an upper bound to determine experimentally the correct demagnetizing current I_{demag} approaching the *remanence coercivity* ($I_{\text{demag}} < I^i_{\text{coer}}$). Due to the numerous non-linear phenomena occurring in the valve, some assumptions are made. Firstly, the iron core is considered a perfect magnetic conductor. Additionally, the MRF flow is considered laminar with a homogeneous particle distribution in the carrier medium. These assumptions lead to the simplified version of Ampere's law:

$$H_{\text{rod}} \cdot l_{\text{rod}} + 2H_{\text{gap}} \cdot g = N \cdot I, \tag{2}$$

with H_{rod}, H_{gap} the magnetic field in the inner rod, and in the gap (i.e. MRF channel) respectively, l_{rod} and g the height of the inner rod, and the width of the gap respectively. The dimensions are shown in Fig. 2 and their values in Table I. The conservation of magnetic flux links the two magnetic flux densities B_{rod}, and B_{gap} in the inner rod and the channel respectively, taking into account the flux fringes:

$$B_{\text{rod}} \cdot \pi r^2_{\text{rod}} = B_{\text{gap}} \cdot 2\pi r_{\text{gap}} \cdot (t_{\text{gap}} + 2 \cdot t_{\text{fr}}), \tag{3}$$

with r_{rod}, the radius of the inner rod and r_{gap} the mean radius of the MRF channel. $t_{\text{gap}} + 2 \cdot t_{\text{fr}}$ is the length of the active region. It includes the length of the gap t_{gap} and the flux fringes t_{fr}. The relationships between the flux density B and the magnetic field H in the materials (AlNiCo-5 and MRF) are non-linear due to saturation effects. A polynomial interpolation of the positive B-H characteristic of the MRF, presented in the MRF132DG datasheet [39], is performed to extract the following relationship:

TABLE II
CURVE FITTING COEFFICIENTS

C_1	$7.40 \cdot 10^{-6}$	α_1	1.498	α_2	1.30
C_2	$-8.51 \cdot 10^{-10}$	β_1	$1.475 \cdot 10^{-7}$	β_2	$7.71 \cdot 10^{-7}$
C_3	$-2.35 \cdot 10^{-10}$	γ_1	-44.56	γ_2	$-5.71 \cdot 10^{-2}$
C_4	$1.86 \cdot 10^{-13}$	δ_1	$-9.01 \cdot 10^{-4}$	δ_2	$-6.20 \cdot 10^{-5}$

$$B_{\text{MRF}(H_{\text{MRF}})} = \sum_{i=1}^{4} C_i \cdot (H_{\text{MRF}})^i. \tag{4}$$

The relationships between the magnetic field and magnetic flux density in the gap can be deduced: $B_{\text{gap}} = B_{\text{MRF}(H_{\text{gap}})}$, and $H_{\text{gap}} = B^{-1}_{\text{MRF}(B_{\text{gap}})}$.

An exponential curve fitting is performed separately for the magnetization and demagnetization parts of the B-H characteristic of the AlNiCo-5 rod obtained experimentally by the German company *Magnet-Physik* (shown in Fig. 3). They are represented with the following equations:

$$B_{\text{AlNiCo\_mag}(H_{\text{AlNiCo}})} = \alpha_1 \cdot e^{\beta_1 \cdot H_{\text{AlNiCo}}} + \gamma_1 \cdot e^{\delta_1 \cdot H_{\text{AlNiCo}}}, \tag{5}$$

$$B_{\text{AlNiCo\_demag}(H_{\text{AlNiCo}})} = \alpha_2 \cdot e^{\beta_2 \cdot H_{\text{AlNiCo}}} + \gamma_2 \cdot e^{\delta_2 \cdot H_{\text{AlNiCo}}}. \tag{6}$$

The coefficients used to interpolate the material properties of the MRF and AlNiCo are shown in Table II. By combining (2), (3), and (4), the current through the coil can be expressed as a function of the magnetic field and magnetic flux density in the magnetic rod $I = I_{(H_{\text{rod}}, B_{\text{rod}})}$:

$$I = \frac{H_{\text{rod}}\, l_{\text{rod}}}{N} + \frac{2g}{N} \cdot B^{-1}_{\text{MRF}} \left(\frac{r^2_{\text{rod}} \cdot B_{\text{rod}}}{2 \cdot r_{\text{gap}} \cdot (t_{\text{gap}} + 2 \cdot t_{\text{fr}})} \right). \tag{7}$$

The current required for a complete magnetization I_{mag} should reach the saturation point of the M-H curve resulting in $I_{\text{mag}} = I_{(H_{\text{sat}}, B_{\text{sat}})}$ with $B_{\text{sat}} = M_{\text{sat}} + \mu_0 H_{\text{sat}}$. As previously stated, the current reaching the *remanence coercivity* of the material cannot be derived analytically. Thus, the current reaching the *intrinsic coercivity* $I^i_{\text{coer}} = I_{(-H^i_{\text{coer}}, -\mu_0 H^i_{\text{coer}})}$ is used, to provide an upper bound to the demagnetization current that will be determined experimentally.

An analytical estimation of the pressure sustained by the valve when closed (i.e. in the no-flow condition) is proposed here. It corresponds to the sum of the field-dependent ΔP_τ and viscosity-dependent ΔP_η pressure drop. It is expressed as follows [21], if flux fringes are not considered:

$$\begin{aligned} \Delta P &= \Delta P_\tau + \Delta P_\eta \\ &= \frac{c \cdot \tau_{(H_{\text{MRF}})} \cdot 2t_{\text{gap}}}{g} + \frac{6 \cdot \eta \cdot Q \cdot 2t_{\text{gap}}}{g^3 \cdot \pi \cdot r_{gap}}, \end{aligned} \tag{8}$$

with Q the flow-rate, η the fluid viscosity, and c a fluid parameter dependent on the ratio $D = \Delta P_\tau / \Delta P_\eta$, which lies between 2 (when $D \approx 1$) and 3 ($D > 100$) [21], [40]. In the case of a closed

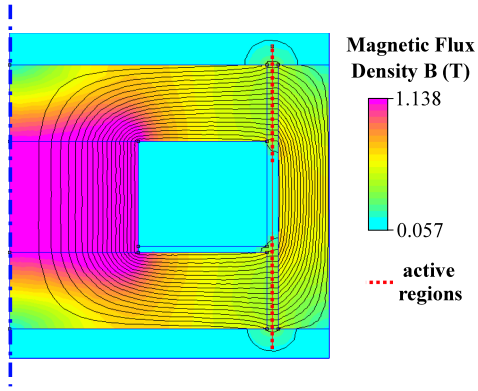

Fig. 4. 2-D axisymmetric simulation of the magnetic flux density in the MRF valve with EPM rod.

valve, $\Delta P_\tau >> \Delta P_\eta$. Thus, the maximum pressure difference sustained by the valve is approximated by $\Delta P_{\max} \approx \Delta P_\tau$, and c lies close to 3. The yield stress function $\tau_{(H_{\mathrm{MRF}})}$ is provided in the datasheet of the MRF [39]. It shows linear characteristics: $B_{\mathrm{MRF}(H_{\mathrm{MRF}})} = aH_{\mathrm{MRF}}$, and $\tau_{(H_{\mathrm{MRF}})} = bH_{\mathrm{MRF}}$ with $a = 0.0047$ and $b = 0.2588$, for $B_{\mathrm{MRF}} < 0.5\,T$.

However, in our case, the quantity of MRF surrounding the valve is big, leading to flux fringes that must be taken into account in our model. The distribution of flux density in the gap is necessary. To this purpose, a 2-D axisymmetric magneto-static simulation of the valve is performed on the *FEMM 4.2* software. It is depicted in Fig. 4, which corresponds to the fully magnetized state of the rod in AlNiCo-5 (using the corresponding B-H characteristic) without current in the coil. The distribution of magnetic flux density along the red dotted line (see Fig. 4) in the gap can thus be evaluated. This allows to reformulate (8) as follows, with l the position in the gap along the aforementioned line:

$$\Delta P_{\max} = \frac{c}{g} \cdot \frac{b}{a} \cdot 2 \cdot \int_{l=0}^{l=t_{\mathrm{gap}}+2\cdot t_{\mathrm{fr}}} B_{\mathrm{MRF}}(l)\, dl. \qquad (9)$$

Although flux fringes are not desirable in magnetic devices, in our case, they lead to the increase of the sustained pressure, improving the capabilities of our device.

III. Experimental Validation

A. Setup and Working Principle

The characteristics of the proposed valve and the key properties of the M-H and B-H characteristics of the AlNiCo-5 are presented in Table I. The total volume V of the valve is 353.25 mm,^{3} which classifies it among the miniaturized versions of valves.

The setup presented in Fig. 5 is used to perform the experimental validation of our device. It constitutes a cylindrical structure with two chambers that are separated by the MR valve. Both chambers 1 and 2 are filled with the MRF (*MRF-132DG* by *Lord Corp.*). Chamber 2 is open and, thus, in atmospheric pressure. A pneumatic piston is inserted into chamber 1. The piston's movement can decrease the volume of chamber 1. This increases the pressure in the latter if the valve is closed, or creates fluid flow if the valve is open. Two pressure sensors (*PFT510 Miniature Pressure Sensor* by *Futek*) measure the pressure in each chamber. A laser displacement sensor (*LK-G3000* by *Keyence*) measures the displacement of the pneumatic piston over time. The coil wires exit chamber 2 and are connected to the electronics that perform valve switching. A current probe (*AP015* by *LeCroy*) is measuring the current flowing in the coil.

Valve activation and deactivation are achieved by applying current pulses to the coil. A positive pulse magnetizes the AlNiCo-5 rod closing the valve, while a smaller negative pulse demagnetizes the rod, opening the valve. A full-bridge arrangement of MOSFETs enables the coil supply with currents in both directions. The *IPB054N08N3-G* MOSFETs from *Infineon Technologies* are used for faster switching (N-channel type), with maximum voltage and current ratings of 80 V and 80 A respectively. Two gate drivers ICs *FAN7842* from *Fairchild Semiconductor Corp.* (one per pair of MOSFETs) are used to drive the gates of the transistors, increasing the switching speed. The gate drivers are controlled with a *F401-RE Nucleo board* from *ST*.

B. Experimental Results

The M-H and B-H characteristics acquired experimentally by the German company *Magnet-Physik* are plotted together in Fig. 6. The light blue curve represents the magnetization M over H and the dark blue curve represents the magnetic flux density B over H. These curves represent the AlNiCo-5 rod from a fully demagnetized condition to the saturation point, after imposing an external field. The third curve in red color represents the demagnetization of the AlNiCo-5 rod, from the fully magnetized condition to $B = 0$. From (7), the current estimated to reach magnetization of the EPM is $I_{\mathrm{mag}} = 7.4$ A. Fig. 6 shows that by decreasing the magnetization current at 5.1 A and, thus, decreasing also the consumed energy, it is possible to reach magnetization close to the saturation M_{sat}. The marked points depicted in Fig. 6 were obtained analytically and numerically according to the simulation of Fig. 4 for the different fixed current values (0 A, 5.1 A, 7.4 A). The analytical and simulation results match with an estimation error less than 6%.

Fig. 7 depicts the voltage across the coil and its measured current during magnetization and demagnetization of the rod. Both actions are achieved with a single current pulse for each one. More specifically, the current for magnetizing the EPM and closing the valve is 5.1 A and is reached within $t_{\mathrm{mag}} = 0.5$ ms. This current value was used experimentally instead of 7.4 A to decrease the power consumption as previously explained. The negative demagnetizing current achieving the *remanence coercivity* (from a fully-magnetized EPM) is determined experimentally: $I_{\mathrm{demag}} = -2.5$ A. One can confirm that it is lower than the upper bound determined analytically ($I_{\mathrm{demag}} < I^i_{\mathrm{coer}}$ = -1.8 A). It is important to point out that the demagnetization of the rod is experimentally determined when the opening of the valve is noticed (i.e. no pressure difference can be sustained). However, perfect demagnetization cannot be assured with this

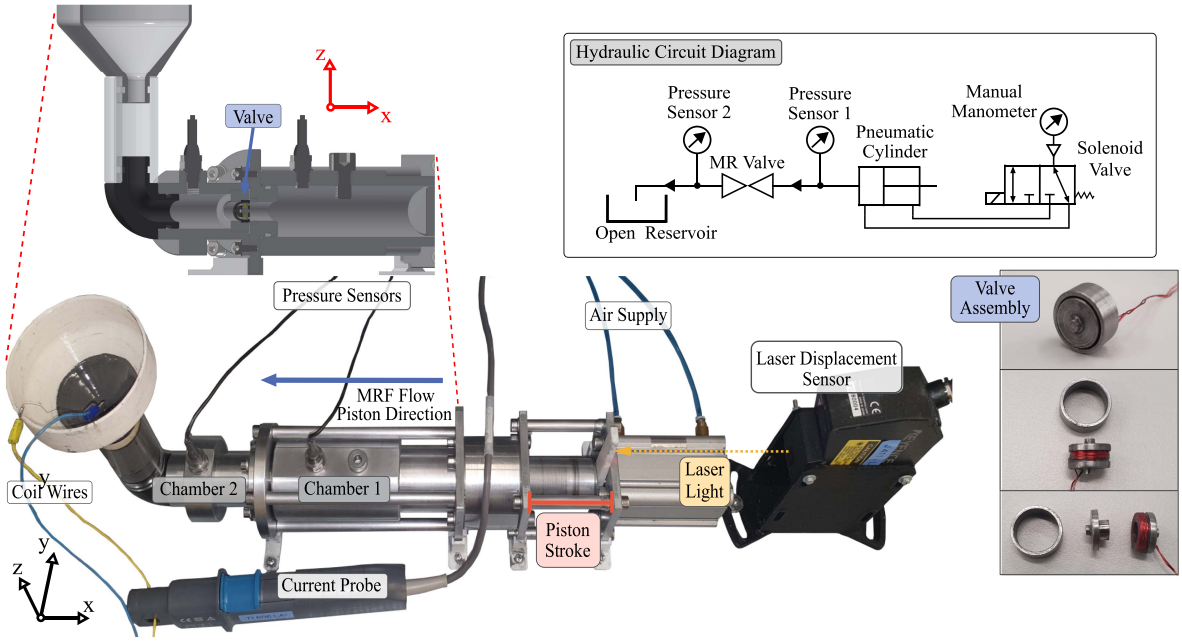

Fig. 5. Experimental setup for the validation of the device and prototype of valve with EPM in the inner rod of the structure. A cut-view of the setup demonstrates the internal part of the chambers, as well as the placement of the valve. The setup is also represented with a hydraulic circuit diagram.

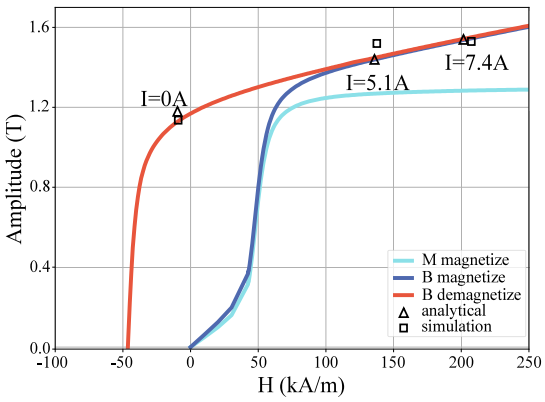

Fig. 6. M-H and B-H characteristics for magnetization, B-H characteristic for demagnetization of the AlNiCo-5 rod, and the B_{rod} and H_{rod} for each current value obtained analytically and with simulation.

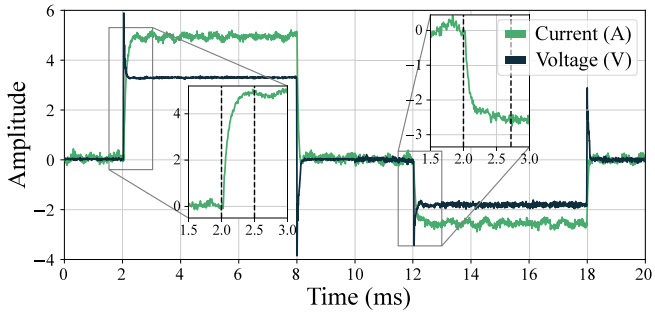

Fig. 7. Pulsed voltage over the coil inside the EPM valve. Positive values result in magnetization of the inner magnetic rod, while negative ones result in its demagnetization.

method. A small magnetization of the rod could still remain while not being strong enough to block the flow in the valve. Nevertheless, in this application, perfect demagnetization of the rod is not critical. The first demagnetization method proposed in Fig. 3 could be used to alleviate this limitation. The demagnetizing current is reached within $t_{\mathrm{demag}} = 0.72$ ms, after the current starts flowing in the coil. Thus, the switching frequency is 0.85 kHz for 50% and 1.25 kHz for 90% duty cycle. These values are high considering different types of fast-switching valves, where switching frequencies are lower than 1 kHz [41], [42]. According to these values, the energy consumption of the valve is 15.3 mJ for activation and 6 mJ for deactivation.

Two experimental scenarios are presented here. The first one studies the comparison between the open and closed condition of the valve. In the closed condition, the rod within the valve is magnetized consecutively with 1.8 A, 3.5 A, and 5.1 A. The piston pressure, and consequently, the pressure in chamber 1, is set and controlled manually with a manometer. The displacement of the piston, as well as the pressure difference between the two sides of the valve (i.e. between chambers 1 and 2) are measured while the piston is moving towards the valve. When the EPM is fully magnetized with 5.1 A, we increase the piston pressure manually with the use of the manometer until our system's limit, which is 1000 kPa. As shown in Fig. 8 (blue plot), there exists an initial abrupt increase of displacement of maximum $\Delta x = 10$ mm, which remains constant as the pressure difference increases. The abrupt increase of displacement at the beginning of the process is explained by the air trapped in the chamber, which is initially compressed. After that, the absence of displacement proves that the valve remains closed. The maximum pressure

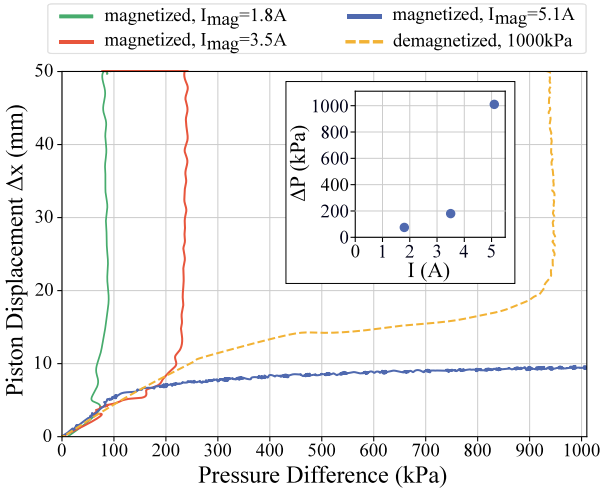

Fig. 8. Piston displacement with respect to the pressure difference between the chambers, for open valve and closed valve with different magnetization currents.

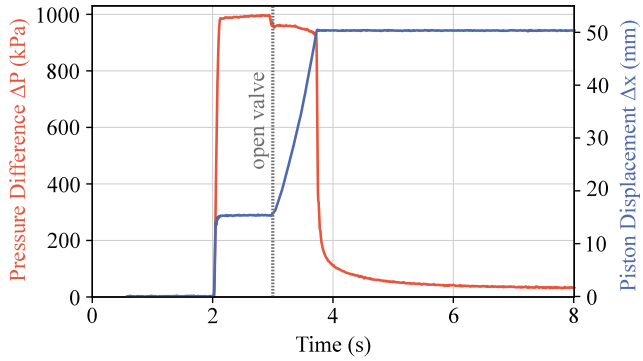

Fig. 9. Pressure difference and piston displacement over time in an EPM valve. The valve is initially closed. At $t = 3\,s$ the demagnetization is taking place and the valve opens, allowing flow and piston displacement.

measured is 1010 kPa. This is the value of pressure that the valve can sustain. Larger pressures could not be tested because the supply of compressed air used for these experiments is limited to 1000 kPa. The value derived from the analytical and simulation results is 949 kPa. The experimental and numerical results match with an estimation error of less than 6.4%.

The proposed system enables the possibility of tuning the sustained pressure. Indeed, the AlNiCo rod could be partially magnetized, and reach lower values than M_{rem} when the current stops. Thus, the magnetic field in the MRF would also be lower, decreasing the pressure that can be sustained. Two additional examples are shown in Fig. 8, with magnetizing currents of 1.8 A and 3.5 A. In the case of $\text{I}_{\text{mag}} = 1.8$ A, the manometer value is set to 100 kPa. At a pressure of 75 kPa, the displacement starts increasing until the stroke limit of 50 mm. In the case of $\text{I}_{\text{mag}} = 3.5$ A, once the air trapped in the chamber is compressed, the displacement also increases to the limit of the system at a pressure of 180 kPa. These results demonstrate the possibility of tuning the sustained pressure. In the open condition, the pressure on the pneumatic piston is again set manually to 1000 kPa. An increase of piston displacement of $\Delta\text{x} = 15$ mm occurs until the pressure measured in chamber 2 reaches 993 kPa. After that the MRF starts flowing with a constant flow rate through the valve. As a result, the piston displacement keeps increasing while the pressure difference remains constant. The piston has a stroke limit of 50 mm. This explains the range of Piston Displacement axis in Fig. 8. The flow rate in this case is calculated as $Q = v \cdot A_{rod} = 459\ \text{mm}^3/\text{s}$, where v is the piston's velocity and A_{rod} is the piston's surface. v is calculated using the experimental measurement of the piston's displacement over time. In (80 is validated with the above experimental values of Q and ΔP, as well as with using $\eta = 0.112\,Pa \cdot s$ from [39] and $\Delta P_\tau = 0$ because the valve is open and there is no magnetic field.

Fig. 9 depicts the second experimental scenario. It shows the displacement Δx of the piston and pressure difference ΔP over time for 1000 kPa of pressure. Switching of the valve from the closed to the open state is demonstrated. The initial condition of the valve is fully-magnetized, after applying the magnetization pulse. At t = 2 s the piston starts pressing and continues for the whole experiment. The valve remains closed until t = 3 s when the demagnetization pulse is applied and the valve is open. During this time there is no piston displacement, except for the initial abrupt displacement that is linked to the air compression. This means that the valve remains closed. When the valve is open, the displacement Δx starts increasing linearly, validating the valve opening. For a pressure difference of 1000 kPa the stroke limit of 50 mm is reached within one second.

IV. Conclusion

Valves constitute an essential component of the control of fluidic power transmission systems. In this letter, we have presented the design, implementation and experimental validation of a miniaturized MRF valve that uses a single-rod EPM. The EPM is magnetized and demagnetized with a single current pulse. The valve can sustain a maximum of 1010 kPa, while it can be activated and deactivated within 0.5 ms and 0.72 ms respectively. In parallel, it consumes negligible power in the steady state condition, with 15.3 mJ for activation and 6 mJ for deactivation. The current work is an improvement compared to the state-of-the-art in terms of power consumption and maximum pressure that can be sustained. Smaller valves exist, however, with much lower capabilities with regard to pressure. Besides, our valve presents the characteristic of tunability of sustained pressure, which can provide flexibility to the applications that use it. Based on these results, our future work will be focused on integrating the current design in robotic applications. Our first goal is to employ the EPM MRF valve in a medical application for plantar pressure offloading in diabetic patients. The MRF valve will be used for the stiffness control of medical footwear.

References

[1] H.-Y. Yang and M. Pan, "Engineering research in fluid power: A review," *J. Zhejiang Univ.- Sci. A*, vol. 16, no. 6, pp. 427–442, 2015.
[2] M. G. El-Din and M. Rabi, Fluid power engineering. New York, NY, USA: McGraw-Hill Education, 2009.

[3] K.-E. Rydberg, "Energy efficient hydraulic hybrid drives," in *Proc. 11th Scand. Int. Conf. Fluid Power*, 2009, pp. 1–14.

[4] H. Shi, H. Yang, G. Gong, H. Liu, and D. Hou, "Energy saving of cutterhead hydraulic drive system of shield tunneling machine," *Automat. Construction*, vol. 37, pp. 11–21, 2014.

[5] S.-H. Hyon, Y. Taniai, K. Hiranuma, K. Yasunaga, and H. Mizui, "Overpressure compensation for hydraulic hybrid servo booster applied to hydraulic manipulator," *IEEE Robot. Automat. Lett.*, vol. 4, no. 2, pp. 942–949, Apr. 2019.

[6] Y. Jiang, J. Ma, D. Chen, Z. Liu, Y. Li, and J. Paik, "Compact pneumatic clutch with integrated stiffness variation and position feedback," *IEEE Robot. Automat. Lett.*, vol. 6, no. 3, pp. 5697–5704, Jul. 2021.

[7] W. Sun, H. Pan, and H. Gao, "Filter-based adaptive vibration control for active vehicle suspensions with electrohydraulic actuators," *IEEE Trans. Veh. Technol.*, vol. 65, no. 6, pp. 4619–4626, Jun. 2016.

[8] Y. Sun, S. Song, X. Liang, and H. Ren, "A miniature soft robotic manipulator based on novel fabrication methods," *IEEE Robot. Automat. Lett.*, vol. 1, no. 2, pp. 617–623, Jul. 2016.

[9] H. K. Yap et al., "A fully fabric-based bidirectional soft robotic glove for assistance and rehabilitation of hand impaired patients," *IEEE Robot. Automat. Lett.*, vol. 2, no. 3, pp. 1383–1390, Jul. 2017.

[10] A. Ainla, M. S. Verma, D. Yang, and G. M. Whitesides, "Soft, rotating pneumatic actuator," *Soft Robot.*, vol. 4, no. 3, pp. 297–304, 2017.

[11] J. W. Booth, J. C. Case, E. L. White, D. S. Shah, and R. Kramer-Bottiglio, "An addressable pneumatic regulator for distributed control of soft robots," in *Proc. IEEE Int. Conf. Soft Robot.*, 2018, pp. 25–30.

[12] G. Gerboni, T. Ranzani, A. Diodato, G. Ciuti, M. Cianchetti, and A. Menciassi, "Modular soft mechatronic manipulator for minimally invasive surgery (MIS): Overall architecture and development of a fully integrated soft module," *Meccanica*, vol. 50, no. 11, pp. 2865–2878, 2015.

[13] C. Chen, W. Tang, Y. Hu, Y. Lin, and J. Zou, "Fiber-reinforced soft bending actuator control utilizing on/off valves," *IEEE Robot. Automat. Lett.*, vol. 5, no. 4, pp. 6732–6739, Oct. 2020.

[14] H. Shi, Z. Liu, H. Wang, and X. Mei, "Design and performance analysis of hydraulic switching valve driven by magnetic shape memory alloy," *Adv. Mech. Eng.*, vol. 13, no. 5, 2021, Art. no. 16878140211016985.

[15] M. C. Carrozza, A. Arena, D. Accoto, A. Menciassi, and P. Dario, "A SMA-actuated miniature pressure regulator for a miniature robot for colonoscopy," *Sensors Actuators A: Phys.*, vol. 105, no. 2, pp. 119–131, 2003.

[16] B. Mosadegh et al., "Integrated elastomeric components for autonomous regulation of sequential and oscillatory flow switching in microfluidic devices," *Nature Phys.*, vol. 6, no. 6, pp. 433–437, 2010.

[17] P. Rothemund et al., "A soft, bistable valve for autonomous control of soft actuators," *Sci. Robot.*, vol. 3, no. 16, 2018, Art. no. eaar7986.

[18] J. Poccard-Saudart, S. Xu, C. B. Teeple, N.-S. P. Hyun, K. P. Becker, and R. J. Wood, "Controlling soft fluidic actuators using soft DEA-based valves," *IEEE Robot. Automat. Lett.*, vol. 7, no. 4, pp. 8837–8844, Oct. 2022.

[19] A. Zatopa, S. Walker, and Y. Menguc, "Fully soft 3D-printed electroactive fluidic valve for soft hydraulic robots," *Soft Robot.*, vol. 5, no. 3, pp. 258–271, 2018.

[20] A. Tonazzini, A. Sadeghi, and B. Mazzolai, "Electrorheological valves for flexible fluidic actuators," *Soft Robot.*, vol. 3, no. 1, pp. 34–41, 2016.

[21] A. Grunwald and A.-G. Olabi, "Design of magneto-rheological (MR) valve," *Sensors Actuators A: Phys.*, vol. 148, no. 1, pp. 211–223, 2008.

[22] F. Imaduddin et al., "A high performance magnetorheological valve with a meandering flow path," *Smart Mater. Structures*, vol. 23, no. 6, 2014, Art. no. 065017.

[23] R. Balak and Y. C. Mazumdar, "Bistable valves for MR fluid-based soft robotic actuation systems," *IEEE Robot. Automat. Lett.*, vol. 6, no. 4, pp. 8285–8292, Oct. 2021.

[24] T.-H. Lee, C. Han, and S.-B. Choi, "Design and damping force characterization of a new magnetorheological damper activated by permanent magnet flux dispersion," *Smart Mater. Structures*, vol. 27, no. 1, 2017, Art. no. 015013.

[25] S. L. Ntella, M.-T. Duong, Y. Civet, Z. Pataky, and Y. Perriard, "Design optimization of miniature magnetorheological valves with self-sensing capabilities used for a wearable medical application," in *Proc. IEEE/ASME Int. Conf. Adv. Intell. Mechatron.*, 2020, pp. 409–414.

[26] A. D. Marchese, C. D. Onal, and D. Rus, "Soft robot actuators using energy-efficient valves controlled by electropermanent magnets," in *Proc. IEEE/RSJ Int. Conf. Intell. Robots Syst.*, 2011, pp. 756–761.

[27] Y. Miyaki and H. Tsukagoshi, "Self-excited vibration valve that induces traveling waves in pneumatic soft mobile robots," *IEEE Robot. Automat. Lett.*, vol. 5, no. 3, pp. 4133–4139, Jul. 2020.

[28] K. Gilpin, A. Knaian, and D. Rus, "Robot pebbles: One centimeter modules for programmable matter through self-disassembly," in *Proc. IEEE Int. Conf. Robot. Automat.*, 2010, pp. 2485–2492.

[29] B. Haghighat, E. Droz, and A. Martinoli, "Lily: A miniature floating robotic platform for programmable stochastic self-assembly," in *Proc. IEEE Int. Conf. Robot. Automat.*, 2015, pp. 1941–1948.

[30] T. Leps et al., "A low-power, jamming, magnetorheological valve using electropermanent magnets suitable for distributed control in soft robots," *Smart Mater. Structures*, vol. 29, no. 10, 2020, Art. no. 105025.

[31] K. J. McDonald, L. Kinnicutt, A. M. Moran, and T. Ranzani, "Modulation of magnetorheological fluid flow in soft robots using electropermanent magnets," *IEEE Robot. Automat. Lett.*, vol. 7, no. 2, pp. 3914–3921, Apr. 2022.

[32] M. R. Jolly, J. D. Carlson, and B. C. Munoz, "A model of the behaviour of magnetorheological materials," *Smart Materials Structures*, vol. 5, no. 5, pp. 607–614, 1996.

[33] A. N. Knaian, "Electropermanent magnetic connectors and actuators: Devices and their application in programmable matter," Ph.D. dissertation, Massachusetts Inst. Technol., Cambridge, MA, USA, 2010.

[34] G. Bertotti, *Hysteresis in Magnetism: For Physicists, Materials Scientists, and Engineers*. New York, NY, USA: Academic Press, May 1998.

[35] F. Thiel, A. Schnabel, S. Knappe-Gruneberg, D. Stollfuss, and M. Burghoff, "Proposal of a demagnetization function," *IEEE Trans. Magn.*, vol. 43, no. 6, pp. 2959–2961, Jun. 2007.

[36] T. Tosun, J. Davey, C. Liu, and M. Yim, "Design and characterization of the EP-Face connector," in *Proc. IEEE/RSJ Int. Conf. Intell. Robots Syst.*, 2016, pp. 45–51.

[37] P. Ward and D. Liu, "Design of a high capacity electro permanent magnetic adhesion for climbing robots," in *Proc. IEEE Int. Conf. Robot. Biomimetics*, 2012, pp. 217–222.

[38] S. Hauser, M. Mutlu, and A. J. Ijspeert, "Kubits: Solid-state self-reconfiguration with programmable magnets," *IEEE Robot. Automat. Lett.*, vol. 5, no. 4, pp. 6443–6450, Oct. 2020.

[39] L. Corporation, "MRF-132DG magneto-rheological fluid," 2022. [Online]. Available: https://lordfulfillment.com/pdf/44/DS7015_MRF-132DGMRFluid.pdf

[40] M. R. Jolly, J. W. Bender, and J. D. Carlson, "Properties and applications of commercial magnetorheological fluids," *J. Intell. Mater. Syst. structures*, vol. 10, no. 1, pp. 5–13, 1999.

[41] H. Wang, Z. Chen, J. Huang, L. Quan, and B. Zhao, "Development of high-speed on–off valves and their applications," *Chin. J. Mech. Eng.*, vol. 35, no. 1, pp. 1–21, 2022.

[42] M. Pan and A. Plummer, "Digital switched hydraulics," *Front. Mech. Eng.*, vol. 13, no. 2, pp. 225–231, 2018.